Chiral-like doublet band structure and octupole correlations in ^{104}Ag

Kaushik Katre,[1,*] P. V. Madhusudhana Rao,[2] R. Raut,[3] A. Sharma,[4] K. Suryanarayana,[2] A. Tejaswi,[2] M. Ratna Raju,[2] D. Vijaya Lakshmi,[2] T. Seshi Reddy,[2] M. Kumar Raju,[5] S. Jehangir,[6] N. Rather,[6] G. H. Bhat,[7] Nazira Nazir,[7] J. A. Sheikh,[7] Y. P. Wang,[8] J. T. Matta,[9] A. D. Ayangeakaa,[10] U. Garg,[11] S. S. Ghugre,[3] T. Trivedi,[12] B. S. Naidu,[13] R. Palit,[13] S. Saha,[14] S. Muralithar,[1] and R. P. Singh[1,†]

[1]*Nuclear Physics Group, Inter-University Accelerator Centre, New Delhi 110067, India*
[2]*Department of Nuclear Physics, Andhra University, Visakhapatnam 530003, India*
[3]*UGC-DAE Consortium for Scientific Research, Kolkata Centre, Kolkata 700098, India*
[4]*Department of Physics, Himachal Pradesh University, Shimla 171005, India*
[5]*Department of Physics, GITAM School of Science, Visakhapatnam 530045, India*
[6]*Department of Physics, Islamic University of Science and Technology, Jammu and Kashmir 192122, India*
[7]*Department of Physics, University of Kashmir, Srinagar 190006, India*
[8]*State Key Laboratory of Nuclear Physics and Technology, School of Physics, Peking University, Beijing 100871, China*
[9]*Physics Division, Oak Ridge National Laboratory, Oak Ridge, Tennessee 37831, USA*
[10]*Department of Physics and Astronomy, University of North Carolina at Chapel Hill, Chapel Hill, North Carolina 27599, USA and Triangle Universities Nuclear Laboratory, Duke University, Durham, North Carolina 27708, USA*
[11]*Department of Physics and Astronomy, University of Notre Dame, Notre Dame, Indiana 46556, USA*
[12]*Department of Pure and Applied Physics, Guru Ghasidas Vishwavidyalaya, Bilaspur 495009, India*
[13]*Department of Nuclear and Atomic Physics, Tata Institute of Fundamental Research, Mumbai 400005, India*
[14]*School of Advanced Sciences, Vellore Institute of Technology, Vellore 632014, India*

(Received 6 May 2022; revised 8 August 2022; accepted 8 September 2022; published 27 September 2022)

The nature of the yrast negative-parity band and its chiral-like partner band in ^{104}Ag is investigated experimentally and theoretically. Lifetimes of states in the negative-parity yrast band and positive-parity band based on the 4424-keV level are measured using Doppler shift attenuation technique. Lifetimes of three more states have been determined along with the upper limit for the lifetime of the highest observed yrast states. Further, lifetimes known from earlier studies are determined with better precision. The level scheme of ^{104}Ag has also been extended with the addition of new enhanced $E1$ transitions linking the positive-parity band based on the 4424-keV levels and the yrast negative-parity and its partner band. $B(E1)$ and/or $B(E1)/B(M1)$ values for the transitions from the positive-parity band to the yrast and its partner band have been determined for the first time; these suggest strong octupole correlation between the positive-parity and the negative-parity bands. Calculations based on the triaxial projected shell model (TPSM) and covariant density functional theory (CDFT) have been performed to unravel the intrinsic structures of the partner band and the excited positive-parity band. TPSM calculations predict that doublet bands have significant angular momentum contributions along the three principle axes, suggesting that bands could have chiral symmetry breaking origin. The CDFT calculations predict a $\pi(g_{9/2})^{-1} \otimes \nu(h_{11/2})(g_{7/2}, d_{5/2})^2$ aligned quasiparticle configuration for the negative-parity doublet bands with deformation parameters $\beta \approx 0.20$ and $\gamma \approx 5^\circ$. The partner band could be interpreted as a chiral vibration mode built on top of the yrast band. The excited positive-parity band is predicted to have aligned four quasiparticle configurations, namely, $\pi(g_{9/2})^{-1} \otimes \nu(h_{11/2})^2 (g_{7/2}, d_{5/2})^1$. Further, these calculations predict significant octupole softness in ^{104}Ag which could be the reason for enhanced $E1$ transitions between the four quasiparticle positive-parity bands and the doublet negative-parity bands.

DOI: 10.1103/PhysRevC.106.034323

I. INTRODUCTION

The structure of nuclei in the $A \approx 100$ region exhibits single-particle and a variety of collective features. The rich band structures observed and the transitions among them render this region an ideal laboratory to test various nuclear structure models and the approximations used therein. Apart from the usual collective rotation of a deformed nucleus, many magnetic rotational (MR) and antimagnetic rotational (AMR) bands have also been reported in nuclei in this region [1–4]. These bands are observed in nuclei near the shell closures having small deformation values. The MR bands are understood as arising from the coupling of neutron and proton angular momenta oriented almost perpendicular to each other

*k_katre@yahoo.com
†rajeshpratap07@gmail.com

at the band head and the generation of angular momentum is due to the alignment of these angular momenta along the rotational axis. This resembles closing of a pair of blades of shears with neutron and proton angular momenta as the blades of the shears, thus these bands are also sometimes referred to as shears bands. AMR bands are interpreted to be arising due to the simultaneous alignment of two (or more) symmetric antialigned proton hole blades along the neutron particle angular momentum, a twin (or more) shears mechanism. Further, the phenomenon of chirality in nuclei, first suggested by Frauendorf and Meng [5], is generally accepted as one of the signatures of triaxial shapes in nuclei and it has been a major focus of recent studies in the $A \approx 100$ region [6–9]. The phenomenon of chirality arises in nuclei due to spontaneous left-right symmetry breaking in triaxial shaped nuclei giving rise to a pair of nearly degenerate bands with identical energy states. These bands in odd-odd triaxial nuclei are thought to arise due to the alignment of angular momentum of the two odd nucleons along the long and the short axis of the nucleus for a hole and particlelike nature, respectively, and the angular momentum of the triaxial core aligned along the intermediate axis, thus giving rise to a left- or a right-handed system in the intrinsic frame of reference, depending on which side of the short-long plane is the total angular momentum vector of the nucleus. However, states in bands of different configurations could also have accidental degeneracy, thus to qualify as true chiral bands the states in the two bands must have very similar physical properties like moment of inertia, quasiparticle alignments, and in-band $B(M1)$ and $B(E2)$ values and $B(M1)/B(E2)$ ratios. Additionally they must also have a smooth energy staggering as a function of spin and a characteristic staggering of in-band and out-of-band $B(M1)/B(E2)$ ratios and energy degeneracy of states at the same spin [10–12].

In many cases, near energy degeneracy of "chiral bands" is observed but the transition probabilities in the two bands are found to be different, as in the case of ^{134}Pr [13] and ^{102}Rh [14]. In the silver isotope ^{106}Ag, chiral-like bands were observed by Joshi *et al.* [10] based on the $\pi g_{9/2}^{-1} \otimes \nu h_{11/2}$ configuration. This is the only case other than the best known candidates for chiral bands in ^{126,128}Cs [15,16] where a crossing is observed between the chiral partners. However, Joshi *et al.* found that the bands have different shapes near the crossover point ($I \approx 14\hbar$). These bands were further investigated by Lieder *et al.* [17] based on lifetime measurements but in conclusion they found that the yrast negative-parity band based on the $\pi g_{9/2}^{-1} \otimes \nu h_{11/2}$ configuration and its proposed partner bands are not chiral partners. In fact, they suggested a different configuration, discussed in detail in the present paper, to the partner band. Wang *et al.* [18] reported observation of chiral doublet bands based on the $\pi g_{9/2}^{-1} \otimes \nu h_{11/2}$ configuration in ^{104}Ag; however, earlier study by Datta *et al.* [19] had found these bands to be magnetic rotational bands. Dar *et al.* [20] analyzed such doublet bands in $A \approx 100$ (including such bands in ^{106,104}Ag) based on the triaxial projected shell model (TPSM) and concluded that these bands have different intrinsic structures. Further, few relatively strong $E1$ transitions were observed from a positive-parity band with the band head at 4424 keV and the yrast negative-parity band. The positive-parity band was suggested to have a four quasiparticle $\pi(g_{9/2})^{-1} \otimes \nu(h_{11/2})^2(g_{7/2}, d_{5/2})$ configuration in Refs. [18,19]. In an effort to have a better understanding of the underlying intrinsic structures and interactions between the bands, lifetime measurements of the levels in the yrast and the excited bands were performed in the present paper. In Sec. II, the details of the experiment are described; Sec. III gives the details of analysis and results including the observation of some new interband and intraband γ transitions; in Sec. IV the results are discussed using the TPSM and covariant density functional theory (CDFT); and finally Sec. V summarizes the present paper.

II. EXPERIMENTAL DETAILS

High-spin excited states of the ^{104}Ag nucleus were populated by using a ^{76}Ge (^{32}S, $p3n\gamma$) ^{104}Ag fusion evaporation reaction at a beam energy of 110 MeV. The ^{32}S beam was delivered by the 14-UD BARC-TIFR Pelletron Facility at Tata Institute of Fundamental Research (TIFR), Mumbai. The target was fabricated by evaporating enriched ^{76}Ge (500 μg/cm^2) on gold foil of thickness 26 mg/cm^2. A thin layer of aluminium (11 μg/cm^2) acting as adhesive was placed between ^{76}Ge and gold foil. The emitted deexciting gamma rays were detected by the Indian National Gamma Array (INGA) consisting of 18 Compton suppressed clover detectors [21]. The clover detectors were placed at six different angles, viz., 40°, 65°, 90°, 115°, 140°, and 157° with respect to the beam direction. Approximately 3.2×10^9 twofold and higher γ-γ coincidence events were collected. The energy and efficiency calibrations were done by using standard ^{152}Eu and ^{133}Ba radioactive sources placed at the target position.

III. DATA ANALYSIS AND RESULTS

A. Level scheme

The data were sorted in γ-γ symmetric and asymmetric matrices by using the MARCOS program [21] and analyzed using RADWARE software packages [22,23]. The symmetric matrix was used to check the published level scheme and to place new gamma rays in the level scheme by generating various gated spectra and the asymmetric matrix was used to determine the multipolarities of the γ-ray transitions from the measurement of the ratio of directional correlation from oriented states ($R_{\rm DCO}$) [24]. The asymmetric matrix with gamma rays detected by detectors at a 140° ring on one axis and gamma rays detected by detectors at 90° on another axis was used to determine DCO ratios and defined as

$$R_{\rm DCO} = \frac{I_\gamma \text{ (observed at 140°, gate on 90°)}}{I_\gamma \text{ (observed at 90°, gate on 140°)}}.$$

The DCO ratios determined for most of the transitions are by using a 346-keV ($10^- \rightarrow 9^-$) γ ray as a gate, the typical value of the DCO ratio for a quadrupole transition was found to be ≈1.6, and for a dipole transition it was ≈1.0. The DCO ratios determined were found consistent with earlier study by Datta *et al.* [19].

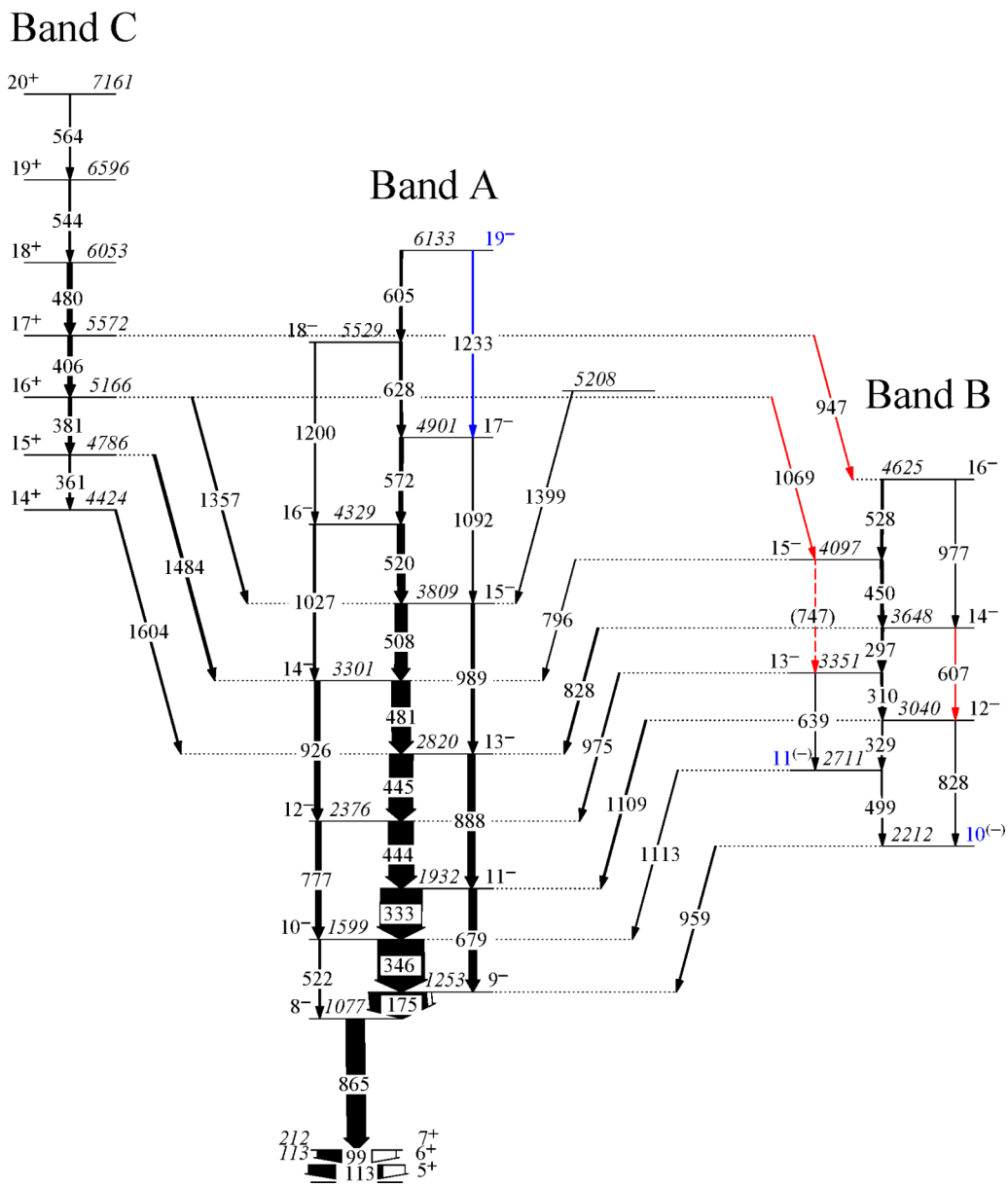

FIG. 1. Partial level scheme of the ^{104}Ag nucleus obtained from the present paper; only γ-ray transitions relevant to the present paper are shown (see text for details). The newly added γ-ray transitions are shown in red color and the confirmed γ-ray transitions or spin/parity are shown in blue color. The widths of the arrows correspond approximately to the intensity of the γ-ray transition.

The partial level scheme of the odd-odd ^{104}Ag nucleus obtained from the present paper is shown in Fig. 1. Gated γ-ray spectra are shown with the gate at 865 keV ($8^- \rightarrow 7^+$, band A) in Fig. 2(a), 406 keV ($17^+ \rightarrow 16^+$, band C) in Fig. 2(b), and 450 keV ($15^- \rightarrow 14^-$, band B) in Fig. 2(c). The level scheme was built on the basis of coincidence relationship, relative intensities, and directional correlation of gamma rays. Most of the γ transitions reported in the earlier studies [18,19] were observed; however, transitions only relevant to the present paper are shown in the partial level scheme in Fig. 1 as listed in Table I. Four new gamma transitions at 947, 1069, 607, and 747 keV were also observed and placed in the level scheme. The details of gamma energies, level energies, initial and final spin states, and $R_{\rm DCO}$ are given in Table I. In the previous study by Wang *et al.* [18] the placement of the 1232.6-keV γ-ray transition, deexciting from the 6133-keV level in the yrast band, was tentative. In the present paper, the placement and spin of $19\hbar$ for the 6133-keV level based on coincidence conditions and DCO ratio measurements of the 605-keV transition are confirmed. The negative parity for the 6133-keV level is because the 1233-keV transition could only be $E2$ since $M2$ or other higher multipolarities are much less likely. Therefore, for this level spin parity adopted is 19^-.

In band B, the $R_{\rm DCO}$ values of 499- and 329-keV transitions deexciting from 2711- and 3040-keV levels, respectively, are found to be close to 1 with a gate on a dipole 175-keV transition with very little mixing [19,25]; thus, the spin assignments of 2711- and 3040-keV levels are confirmed, however parities

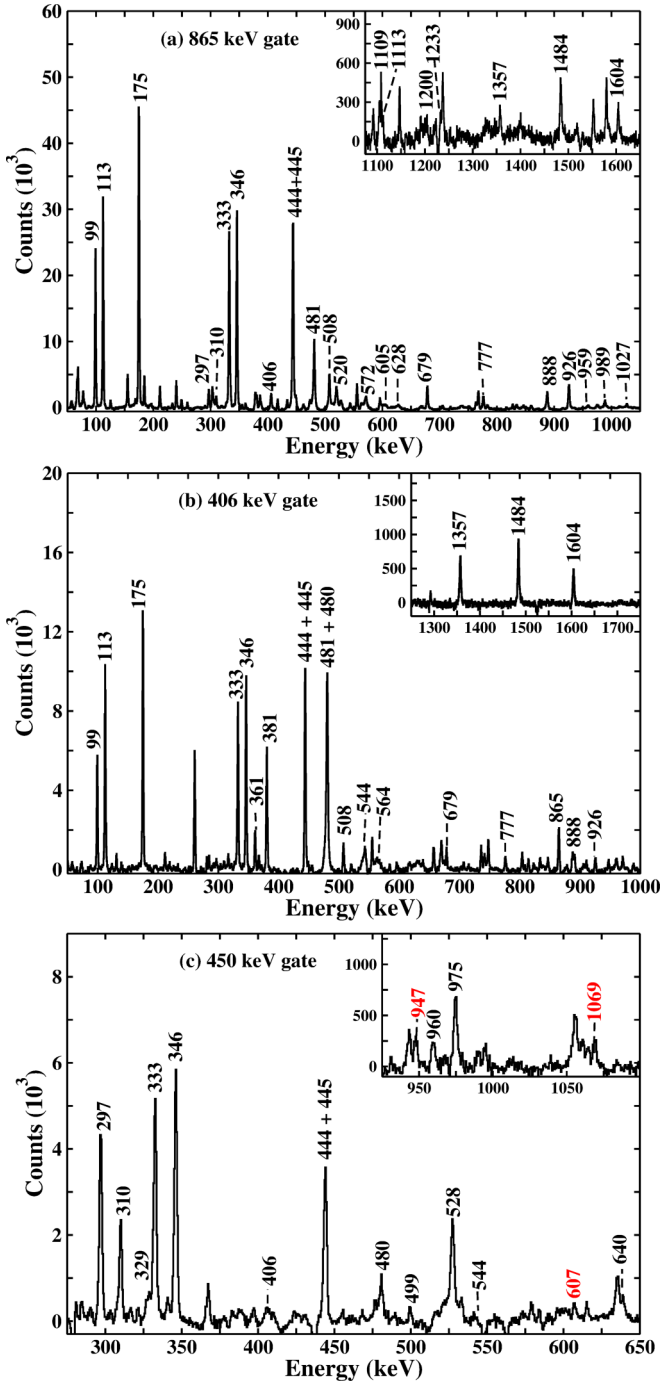

FIG. 2. γ-γ coincidence spectra with the (a) 865-, (b) 406-, and (c) 450-keV gates belonging to band *A*, band *C*, and band *B*, respectively. The newly observed γ transitions from the present paper are shown with energy in red color.

are still kept tentative following the adoption by Wang *et al.* [18]. A new transition (607 keV) deexciting from the level at 3648 keV to the level at 3040 keV was observed and is placed in the level scheme. Two new $E1$ transitions from band *C* to band *B* from 17^+ to 16^- (947 keV) and from 16^+ to 15^- (1069 keV) were also observed and are placed in the level scheme. These new transitions can be seen in Fig. 2(c) in the gated spectra with the gate on the 450-keV ($15^- \rightarrow 14^-$) transition in band *B* with E_γ marked in red color. Other gated γ spectra are also shown in Figs. 2(a) and 2(b).

B. Level lifetime analysis using the Doppler shift attenuation method

Doppler shift attenuation method (DSAM) analysis was carried out to extract lifetimes of excited states of band *A* and band *C*. Data were sorted into angle dependent asymmetric matrices, with the γ rays observed at one of the four (40°, 65°, 140°, and 157°) possible angles on the *y* axis and coincident γ rays detected at the 90° on the *x* axis. The analysis was carried out by using the LINESHAPE [26] package together with developments reported in Ref. [27]. The same is merited with the use of stopping powers of SRIM [28] software for simulation of residue trajectories through target and backing media, which thus reduces systematic uncertainty on the lifetime results from the use of older stopping power models as implemented in the LINESHAPE package. As per the routine procedure of the DSAM analysis, the calculated Doppler-broadened line shapes were least square fitted to the experimental spectra at different angles in order to determine the lifetime of the respective level. The detailed methodology is described in a number of papers such as Ref. [29]. The parameters of fitting include the level lifetime, the side feeding lifetime, the spectrum background, and the height of the transition peak along with that of the neighboring contamination peak, if any. For each level of interest, a single feeder state was used to model the side feeding contribution to the observed experimental γ-ray transition peak. During the analysis χ^2 minimization was carried out for experimental spectra beginning from the topmost level which was assumed to be 100% side fed. Lifetime of the level, the side feeding time, and other parameters were allowed to vary for converging into a χ^2 minimum. In the second step, the side feeding time and the lifetime of levels were allowed to vary simultaneously while keeping the other (spectrum) parameters of individual states fixed at the values obtained in the previous steps. The lifetimes corresponding to those arrived at from this global minimization were the final values quoted herein.

In the present DSAM analysis both spectra generated with the gate on the transition below (GTB) as well as spectra with the gate on the transition above (GTA) the transition of interest wherever feasible are used. One of the spectra corresponding to the GTB was generated by summing gates on 346-, 333-, and 444-keV transitions of the yrast band (band *A*). Lifetimes of the states 15^-, 16^-, 17^-, 18^-, and 19^- belonging to band *A* were extracted from analysis of this spectrum. The experimental spectra along with fitted Doppler shapes at four different angles for some of these deexciting transitions are shown in Figs. 3(a) and 3(b). Lifetimes of the 16^+ and the 17^+ states of band *C* were also extracted from analysis of the same spectrum with GTB.

As far as the present data are concerned, no Doppler shapes were observed for transitions deexciting the 14^+ and the 15^+ states of band *C*. Given that the stopping time of the ^{104}Ag residues in the target and backing media for the experiment is $\approx$1.3 ps, not observing the Doppler shape for these transitions

TABLE I. γ energy (E_γ), level energy (E_i), relative intensity (I_γ), and $R_{\rm DCO}$ of the γ transitions in ^{104}Ag obtained from the gate on pure dipole 346-keV transition.

E_γ (keV)[a]	E_i (keV)	$J_i^\pi \rightarrow J_j^\pi$	Intensity I_γ	DCO ratio $R_{\rm DCO}$
99.3	212	$7^+ \rightarrow 6^+$	120.6(60)	
112.6	113	$6^+ \rightarrow 5^+$	162.9(81)	
175.2	1253	$9^- \rightarrow 8^-$	126.0(63)	0.95(1)
297.2	3648	$14^- \rightarrow 13^-$	5.1(3)	1.06(8)
310.1	3351	$13^- \rightarrow 12^-$	3.7(2)	1.06(11)
328.9	3040	$12^- \rightarrow 11^{(-)}$	1.7(1)	1.07(11)[b]
332.8	1932	$11^- \rightarrow 10^-$	89.6(45)	1.01(3)
346.3	1599	$10^- \rightarrow 9^-$	100.0(50)	1.13(1)[c]
361.4	4786	$15^+ \rightarrow 14^+$	2.9(2)	0.91(9)
380.8	5166	$16^+ \rightarrow 15^+$	7.3(4)	0.99(12)
406.1	5572	$17^+ \rightarrow 16^+$	9.9(5)	0.92(5)
443.8	2376	$12^- \rightarrow 11^-$	53.9(52)	0.99(1)
444.7	2820	$13^- \rightarrow 12^-$	50.9(25)	0.99(1)
449.6	4097	$15^- \rightarrow 14^-$	5.8(3)	0.90(7)
480.1	6053	$18^+ \rightarrow 17^+$	10.5(5)	
481.2	3301	$14^- \rightarrow 13^-$	40.3(20)	1.02(2)
499.3	2711	$11^{(-)} \rightarrow 10^{(-)}$	1.6(3)	1.02(14)[b]
507.8	3809	$15^- \rightarrow 14^-$	26.4(13)	0.93(2)
519.8	4329	$16^- \rightarrow 15^-$	15.6(8)	0.90(5)
521.7	1599	$10^- \rightarrow 8^-$	3.7(2)	
527.6	4625	$16^- \rightarrow 15^-$	4.8(2)	1.08(11)
543.6	6596	$19^+ \rightarrow 18^+$	2.9(2)	
564.2	7161	$20^+ \rightarrow 19^+$	2.7(2)	
572.3	4901	$17^- \rightarrow 16^-$	7.9(4)	0.90(6)
604.8	6133	$19^- \rightarrow 18^-$	4.8(3)	0.91(9)
606.6	3648	$14^- \rightarrow 12^-$	0.6(2)	
627.7	5529	$18^- \rightarrow 17^-$	5.5(3)	1.00(13)
638.9	3351	$13^- \rightarrow 11^{(-)}$	0.7(1)	
678.9	1932	$11^- \rightarrow 9^-$	17.4(9)	1.55(3)[c]
746.7	4097	$15^- \rightarrow 13^-$	$\leqslant 1$	
776.7	2376	$12^- \rightarrow 10^-$	12.3(6)	1.64(8)
796.2	4097	$15^- \rightarrow 14^-$	0.7(1)	
827.7	3040	$12^- \rightarrow 10^{(-)}$	0.8(2)	
828.1	3648	$14^- \rightarrow 13^-$	3.4(2)	1.13(8)
865.2	1077	$8^- \rightarrow 7^+$	40.6(21)[d]	
888.4	2820	$13^- \rightarrow 11^-$	15.5(8)	1.56(13)
925.8	3301	$14^- \rightarrow 12^-$	11.2(6)	1.49(14)
946.9	5572	$17^+ \rightarrow 16^-$	1.0(1)	
959.3	2212	$10^{(-)} \rightarrow 9^-$	2.4(2)	
975.3	3351	$13^- \rightarrow 12^-$	2.6(2)	1.03(18)
977.1	4625	$16^- \rightarrow 14^-$	1.0(2)	
989.0	3809	$15^- \rightarrow 13^-$	7.6(4)	1.40(7)
1027.3	4329	$16^- \rightarrow 14^-$	4.9(3)	
1069.4	5166	$16^+ \rightarrow 15^-$	1.0(1)	
1091.8	4901	$17^- \rightarrow 15^-$	2.2(1)	
1108.9	3040	$12^- \rightarrow 11^-$	3.3(2)	1.09(10)
1112.9	2711	$11^{(-)} \rightarrow 10^-$	1.5(1)	
1200.1	5529	$18^- \rightarrow 16^-$	2.1(3)	
1232.6	6133	$19^- \rightarrow 17^-$	1.8(3)	
1357.4	5166	$16^+ \rightarrow 15^-$	3.1(2)	1.10(33)
1399.3	5208	$\rightarrow 15^-$	1.1(1)	
1484.4	4786	$15^+ \rightarrow 14^-$	5.2(3)	0.88(12)
1604.4	4424	$14^+ \rightarrow 13^-$	3.0(2)	1.04(25)

[a]The uncertainty in γ-ray energy is within 0.5 keV and the level energies are rounded off to the nearest integer value.
[b]DCO ratio from the gate on the 175-keV dipole transition.
[c]DCO ratio from the gate on the 444-keV dipole transition.
[d]The level at 1077 keV deexcites by other transitions to lower levels as reported in Ref. [18]; these were observed in the present paper but not listed in this table.

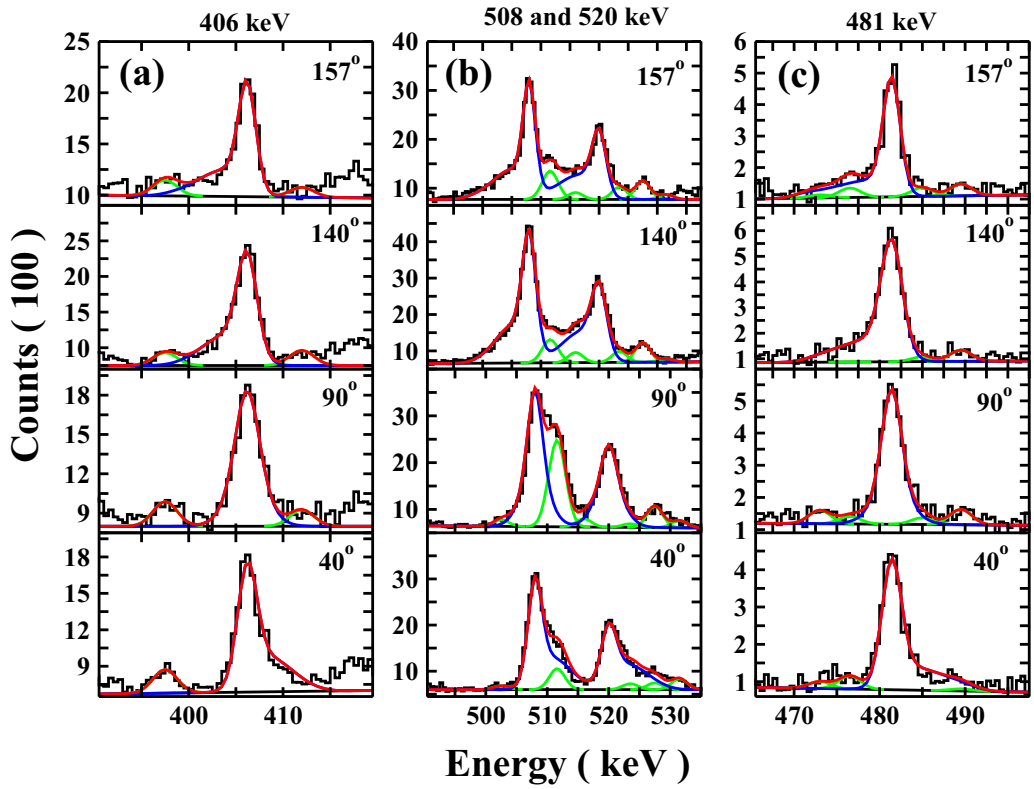

FIG. 3. The experimental spectra along with the fitted line shapes for the 406-, 508-, 520-, and 481-keV γ transitions of band A and C. The line shapes of the γ transition, contamination peaks, and total line shape are shown by blue, green, and red curves, respectively.

would mean that the lifetimes of the corresponding levels are >4 ps. This is consistent with the propositions of Datta *et al.* [19]. The lifetime of the 16^+ and 17^+ states, as mentioned earlier, could be determined from the analysis of the GTB spectrum corresponding to the sum gates on 346-, 333-, and 444-keV transitions of band A. The lifetimes of the still higher (18^+ and 19^+) states of band C were extracted from analysis of another GTB spectrum generated from the sum of gates on 361-, 1604-, 1484-, 926-, and 989-keV transitions. The choice of gates was such that there was no contribution of the 481-keV ($14^- \rightarrow 13^-$) transition in the observed Doppler shape of the 480-keV ($18^+ \rightarrow 17^+$) transition peak of band C, because in this selection of gates the 481-keV transition of band A is being contributed only by the 1484-keV transition deexciting the long-lived 15^+ state of band C. Thus, the 481-keV transition peak could be defined as a stopped contaminant one in the analysis of the Doppler shape of the 480-keV transition.

The $B(E1)/B(M1)$ and $B(E1)$ values determined for transitions from band C to band A and band B are given in Table III.

Lifetimes of some of the states of band A could also be determined from analysis of the spectrum corresponding to a GTA the levels of interest. Such analysis is known to eliminate the uncertainties associated with the side feeding, albeit the count statistics in the GTA spectra is often sparse and the technique cannot be practiced at large. In the present analysis, a gate on the 572-keV ($17^- \rightarrow 16^-$) transition was used to determine the lifetimes of the 14^-, 15^-, and 16^- levels of band A, that are respectively deexcited by the 481-, 508-, and 520-keV transitions. The fitted line shapes to the experimental spectra at four different angles for the 481-keV deexciting transition are shown in Fig. 3(c). The extracted lifetimes of 14^-, 15^-, and 16^- states have been tabulated in Table II. The lifetime values obtained for the 15^- and 16^- states are in superior overlap with these obtained from the previous analysis using the spectrum corresponding to the GTB. This provides a validation for the latter. The uncertainties on lifetime values have been calculated from χ^2 analysis added in quadrature to the systematic contribution of the stopping powers, that is, ≈5% [28].

The reduced transitional probability was calculated from the measured level lifetime τ, using [30]

$$B(M1)\downarrow = \frac{0.056\,97 B_\gamma(M1)}{E_\gamma^3(M1)\tau[1+\alpha_t(M1)]}[(\mu_N)^2] \qquad (1)$$

where $\alpha_t(M1)$ is the total internal conversion coefficient of the transition and $B_\gamma(M1)$ is the branching ratio. The E_γ in the above expression is in MeV and τ is in picoseconds. We have assumed the values of the mixing ratio to be negligible to estimate the $B(M1)$ values. Further, for $E_\gamma > 300$ keV the total internal conversion coefficient of the transition $\alpha_t(M1)$ is found to be negligible.

IV. DISCUSSION

In the study by Datta *et al.* [19] the yrast band A and band B (Fig. 1) were assigned the $\pi(g_{9/2})^{-1} \otimes \nu(h_{11/2})(g_{7/2}, d_{5/2})^2$

TABLE II. Spin (I^π), γ energy (E_γ), level energy, measured level lifetime from the present paper using the GTB ($\tau_{\rm GTB}$), side feeding lifetime obtained from GTB technique ($\tau_{\rm SF}$), level lifetime obtained using GTA ($\tau_{\rm GTA}$) technique, adopted lifetime (τ), and the reduced transition probabilities $B(M1)$ for band A and band C.

I^π ($\hbar$)	E_γ (keV)	Level energy (keV)	$\tau_{\rm GTB}$ (ps)	$\tau_{\rm SF}$ (ps)	$\tau_{\rm GTA}$ (ps)	Adopted τ (ps)	$B(M1)\downarrow$ μ_N^2	$B(M1)\downarrow$ (W.u.)
Band A								
14^-	481.2	3301			$0.52^{+0.06}_{-0.06}$	$0.52^{+0.06}_{-0.06}$	$0.76^{+0.09}_{-0.09}$	$0.42^{+0.05}_{-0.05}$
15^-	507.8	3809	$0.37^{+0.05}_{-0.05}$	$0.43^{+0.05}_{-0.05}$	$0.40^{+0.06}_{-0.05}$	$0.40^{+0.06}_{-0.05}$	$0.85^{+0.13}_{-0.11}$	$0.47^{+0.07}_{-0.06}$
16^-	519.8	4329	$0.37^{+0.05}_{-0.05}$	$0.35^{+0.05}_{-0.05}$	$0.37^{+0.06}_{-0.06}$	$0.37^{+0.06}_{-0.05}$	$0.83^{+0.13}_{-0.11}$	$0.46^{+0.07}_{-0.06}$
17^-	572.3	4901	$0.25^{+0.05}_{-0.05}$	$0.31^{+0.06}_{-0.05}$		$0.25^{+0.05}_{-0.05}$	$0.95^{+0.19}_{-0.19}$	$0.53^{+0.11}_{-0.11}$
18^-	627.7	5529	$0.29^{+0.05}_{-0.05}$	$0.19^{+0.08}_{-0.05}$		$0.29^{+0.05}_{-0.05}$	$0.58^{+0.10}_{-0.10}$	$0.32^{+0.06}_{-0.06}$
19^-	604.8	6133	0.68 $\downarrow$			0.68 $\downarrow$	0.28 $\uparrow$	0.16 $\uparrow$
Band C								
16^+	380.8	5166	$0.61^{+0.05}_{-0.05}$	$0.79^{+0.06}_{-0.06}$		$0.61^{+0.05}_{-0.05}$	$1.08^{+0.09}_{-0.09}$	$0.60^{+0.05}_{-0.05}$
17^+	406.1	5572	1.34 $\downarrow$			1.34 $\downarrow$	0.58 $\uparrow$	0.32 $\uparrow$
18^+	480.1	6053	$0.39^{+0.05}_{-0.05}$	$0.41^{+0.05}_{-0.05}$		$0.39^{+0.05}_{-0.05}$	$1.31^{+0.17}_{-0.17}$	$0.73^{+0.09}_{-0.09}$
19^+	543.6	6596	0.86 $\downarrow$			0.86 $\downarrow$	0.41 $\uparrow$	0.23 $\uparrow$

configuration with the neutron quasiparticle in favored and unfavored orbits of the $h_{11/2}$ orbital, respectively, based on cranked shell model calculations. These bands were further proposed to be magnetic rotational bands. Wang *et al.* [18] claimed that band A and band B were chiral partner bands based on the $\pi(g_{9/2})^{-1} \otimes \nu(h_{11/2})$ configuration; however, it was also stated that more experimental data were required to confirm this conclusion. The positive-parity band C was also assigned to be a magnetic rotational band in Ref. [19] using tilted axis cranking calculations and in Ref. [18] this band was assigned a four quasiparticle configuration $\pi(g_{9/2})^{-1} \otimes \nu(h_{11/2})^2(g_{7/2}, d_{5/2})^1$ based on comparison to four quasiparticle bands in neighboring ^{106}Ag [31] and ^{108}Ag [32] silver isotopes.

The $E1$ transitions from the positive-parity band C to the negative-parity bands are significantly strong as is evident from Table III with high $B(E1)$ values ($\approx 10^{-4}$ W.u., where W.u. denotes Weisskopf units). In ^{109}Te, de Angelis *et al.* [33] had reported strong $E1$ transitions with similar $B(E1)$ values between bands with $(h_{11/2})^2(g_{7/2}, d_{5/2})^1$ and $(h_{11/2})(g_{7/2}, d_{5/2})^2$ configurations in ^{109}Te. These were ascribed to strong octupole correlations due to the mixing of configurations induced by rotation. It is to be noted that such strong octupole correlations have been observed in ^{108}Te [34], ^{114}Xe [35], ^{117}Xe [36], and ^{124,125}Cs [37] nuclei close to the $A \approx 100$ region similar to those reported in ^{124,125}Ba [38].

To better understand the above band structures and the measured transition probabilities, we have carried out TPSM and CDFT calculations. Predictions of these models and their comparison with the data are described below.

A. Triaxial projected shell model results

In recent years, the TPSM approach has been demonstrated to reproduce the high-spin properties of well deformed and transitional nuclei reasonably well [39,40]. In particular, it has been shown that it reproduces the properties of doublet bands observed in odd-odd [41], odd-mass [42], and even-even [39] systems quite well. In the earlier version, the basis space in the TPSM approach for odd-odd nuclei was composed of one-neutron coupled to one-proton quasiparticle configurations [43]. This basis space was obviously quite restrictive and allowed one to study only low-lying states in odd-odd nuclei. To study the high-spin states in odd-odd nuclei around and beyond the band crossing, it is important to include two-neutron and two-proton states coupled to the basic one-neutron plus one-proton state. These basis states have been recently included in the TPSM approach and already some studies have been performed [41]. In order to investigate the properties of ^{104}Ag, the TPSM basis states have been constructed with the basis deformation of $\epsilon = 0.142$ and $\epsilon' = 0.100$, which correspond to quadrupole deforma-

TABLE III. Spin (I^π), γ energy (E_γ), branching ratio, $B(E1)/B(M1)$ values, and the reduced transition probabilities $B(E1)$.

I^π ($\hbar$)	$E_\gamma(E1)$ (MeV)	Br.	$B(E1)/B(M1)$ (10^{-4} efm/μ_N)^2	$B(E1)\downarrow$ (10^{-5} W.u.)
15^+	1.484	0.64	$2.84^{+0.25}_{-0.25}$	
16^+	1.357	0.27	$1.03^{+0.09}_{-0.09}$	$7.84^{+0.64}_{-0.64}$
	1.069	0.09	$0.68^{+0.08}_{-0.08}$	$5.34^{+0.44}_{-0.44}$
17^+	0.947	0.09	$0.88^{+0.10}_{-0.10}$	3.50 $\uparrow$

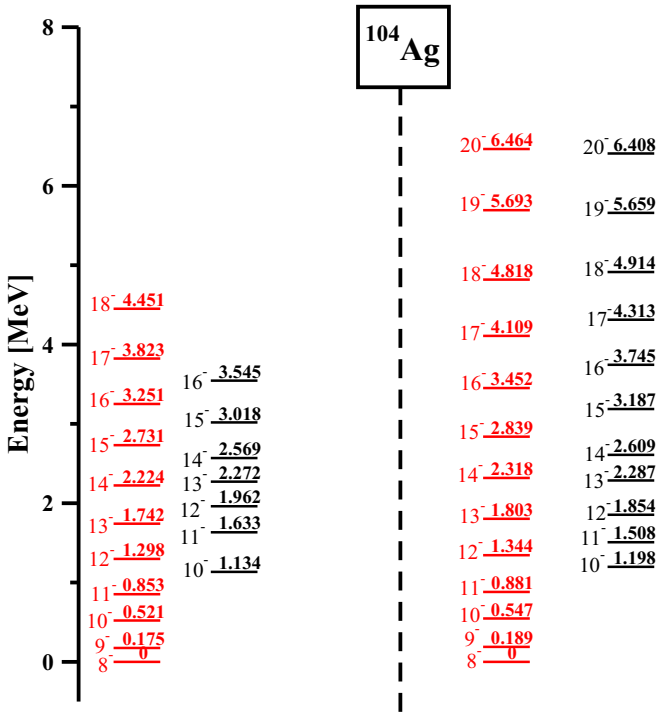

FIG. 4. Comparison of the measured energy levels of negative-parity yrast and excited bands for the ^{104}Ag nucleus (left side) with the results of TPSM calculation (right side).

tion $\beta \approx 0.15$ and $\gamma \approx 35^\circ$ [19,44]. The deformed triaxial basis generated is projected onto good angular momentum states through three-dimensional (3D) angular momentum projection formalism [45]. The projected basis is then employed to diagonalize the shell model Hamiltonian consisting of pairing plus quadrupole-quadrupole interaction terms. The projected energies obtained after shell model diagonalization for the ^{104}Ag odd-odd nucleus are depicted and compared with the corresponding experimental data in Fig. 4. It is evident from the figure that overall agreement between the calculated and the measured energies is quite reasonable. In order to shed light on the possibility that two observed negative bands may be associated with the chiral symmetry breaking mechanism, we have calculated the angular momentum projections along the three principle axes. As is well known, chiral symmetry results in a triaxial system, having finite angular momentum projection along all the three principle axes. The angular momentum projections are plotted in Fig. 5 for the two doublet bands, and it is evident from the results that three axes have finite angular momentum projections. This suggests that two negative-parity observed bands could be associated with the chiral symmetry. Similar analysis has recently been carried out for ^{104}Mo in Ref. [48], and more details on the calculations can be found in the cited article.

In Fig. 6 the experimental kinematic moment of inertia is compared with the calculated moment of inertia for bands A and B. The Harries parameters used are $\mathrm{Im}_0 = 7.0\hbar^2/\mathrm{MeV}$ and $\mathrm{Im}_1 = 15.0\hbar^4/\mathrm{MeV}$ [46]. The moments of inertia for the two bands are quite different at spins below $15\hbar$, however they tend to become similar at higher spins. The transition probabilities have also been evaluated using the projected wave functions after diagonalization with the expressions given in Ref. [43]. The parameters of $g_l^\pi = 1$, $g_l^\nu = 0$, $g_s^\pi = 5.586 \times$

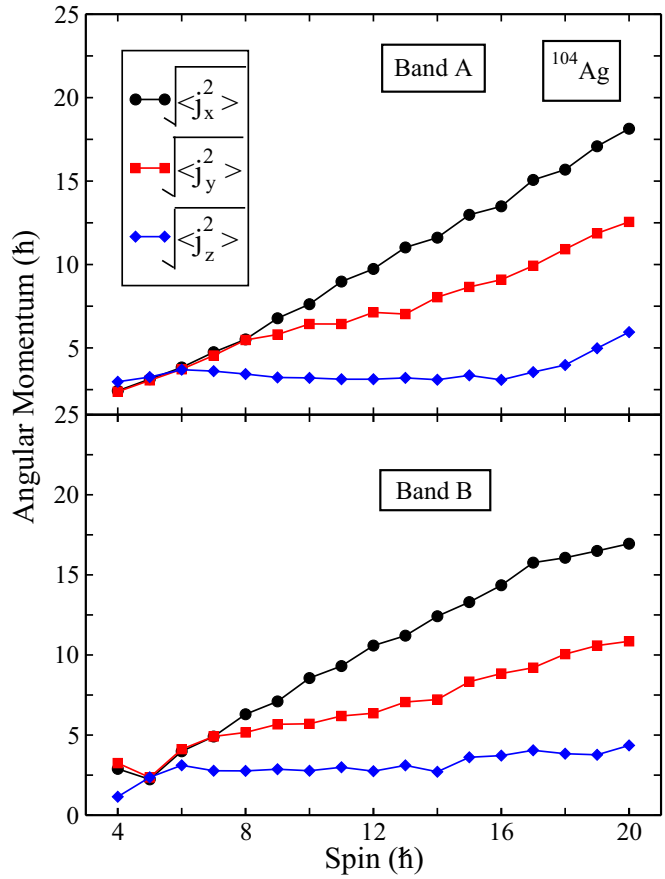

FIG. 5. The expectation values of the squared angular momentum components in band A and band B for the nucleus ^{104}Ag.

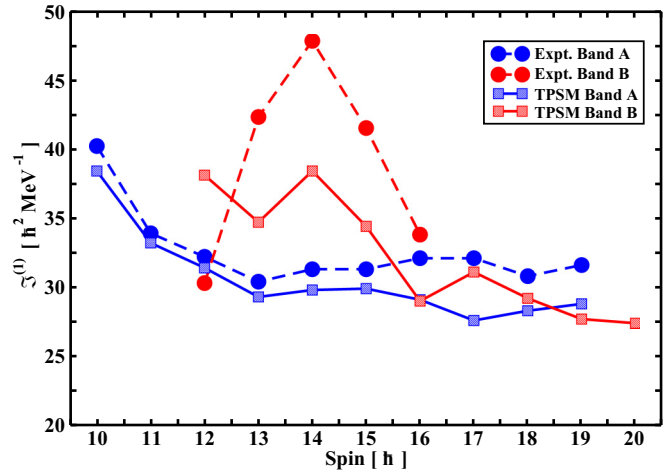

FIG. 6. Comparison between experimental and calculated moments of inertia $J^{(1)}$ of the yrast band and partner band for ^{104}Ag. The Harries parameters used are $\mathrm{Im}_0 = 7.0\ \hbar^2/\mathrm{MeV}$ and $\mathrm{Im}_1 = 15.0\ \hbar^4/\mathrm{MeV}$ [46].

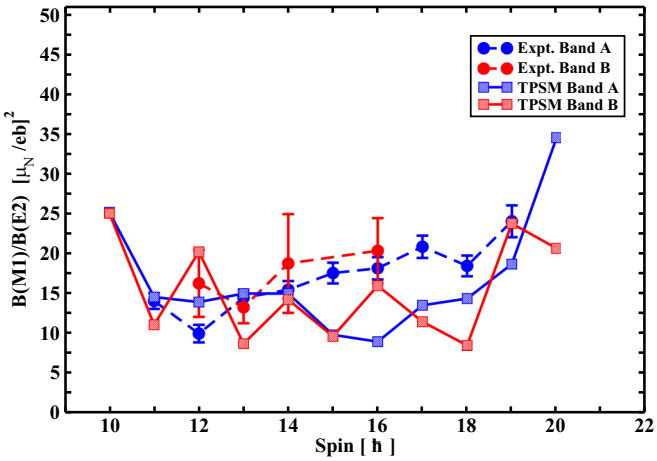

FIG. 7. Comparison of the experimental and theoretical $B(M1)/B(E2)$ ratios for ^{104}Ag.

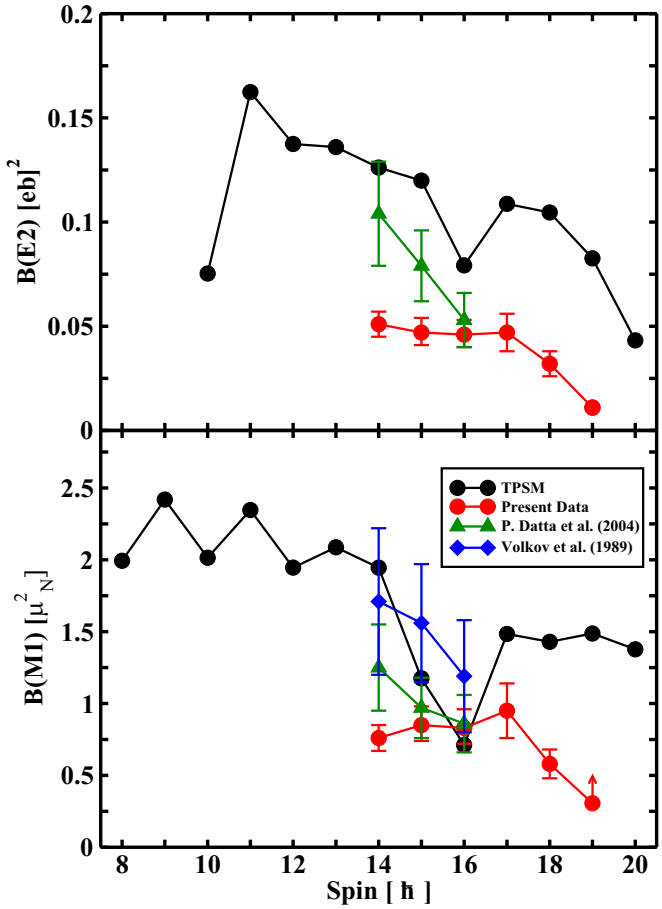

FIG. 8. Comparison of the experimental and theoretical $B(M1)$ and $B(E2)$ for band A of the ^{104}Ag nucleus. The error depicted for the present paper includes error in stopping power ≈5% (the error bars shown for data points from the previous studies [19,47] do not include the stopping power error).

0.85, and $g_s^\nu = -3.826 \times 0.85$ and the effective charges of $e^\pi = 1.5e$ and $e^\nu = 0.5e$ have been employed as in our earlier work [43]. It is evident from Fig. 7 that $B(M1)/B(E2)$ ratios of the yrast and the partner band are in good agreement with the experimental data. The calculated transition probabilities $B(M1)$ and $B(E2)$ vs spin are compared with the experimental data in Fig. 8. Individual calculated values are compared with the known values from various experimental measurements [19,47]. The TPSM calculated $B(E2)$ values are slightly higher than the measured ones. To investigate positive-parity states in ^{104}Ag, the TPSM approach needs to be generalized to include two major shells for the valence space. This development is presently under progress and the results will be published in a separate communication.

B. Covariant density functional theory results

To understand the structure of the bands in ^{104}Ag, calculations based on the CDFT [49–51] have been carried out. The energy spectra, angular momenta, and electromagnetic transition probabilities have been calculated by the three-dimensional cranking covariant density functional theory (3DTAC-CDFT) [52–54]. The octupole deformation of the ground state in ^{104}Ag has been examined based on CDFT in a 3D lattice [55–57]. The relativistic density functional PC-PK1 [58] is used, which has demonstrated high predictive power to describe nuclear masses [59–61], magnetic and antimagnetic rotations [62–64], chiral rotations [52], etc. For the 3DTAC-CDFT calculation, the Dirac equation is solved in a 3D harmonic oscillator basis in Cartesian coordinates with ten major shells which provide convergent results for nuclei in the $A \approx 100$ mass region [52]. The configuration-fixed constrained triaxial CDFT calculations similar to those in Ref. [65] were performed for various low-lying particle-hole excitations in ^{104}Ag. Detailed results are listed in Table IV. Three positive-parity configurations are labeled as $\alpha+$, $\beta+$,

TABLE IV. Binding energies, deformations β and γ, and the corresponding configurations for the minima $\alpha+$, $\beta+$, $\gamma+$, $\alpha-$, and $\beta-$ in ^{104}Ag obtained in the configuration-fixed 3DTAC-CDFT calculations with PC-PK1.

State	E (MeV)	β	γ	Configurations
$\alpha+$	886.9	0.189	0.0°	$\pi\left(g_{9/2}^{-3}\right) \otimes \nu(g_{7/2}, d_{5/2})^7$
$\beta+$	883.7	0.240	7.5°	$\pi\left(g_{9/2}^{-3}\right) \otimes \nu\left(h_{11/2}^{2}\right)(g_{7/2}, d_{5/2})^5$
$\gamma+$	884.5	0.220	19.4°	$\pi\left(g_{9/2}^{-2}\right)(p_{1/2}, p_{3/2})^{-1} \otimes \nu\left(h_{11/2}^{1}\right)(g_{7/2}, d_{5/2})^6$
$\alpha-$	885.7	0.220	0.0°	$\pi\left(g_{9/2}^{-3}\right) \otimes \nu\left(h_{11/2}^{1}\right)(g_{7/2}, d_{5/2})^6$
$\beta-$	883.4	0.242	39.0°	$\pi\left(g_{9/2}^{-1}\right)(p_{1/2}, p_{3/2})^{-2} \otimes \nu\left(h_{11/2}^{1}\right)(g_{7/2}, d_{5/2})^6$

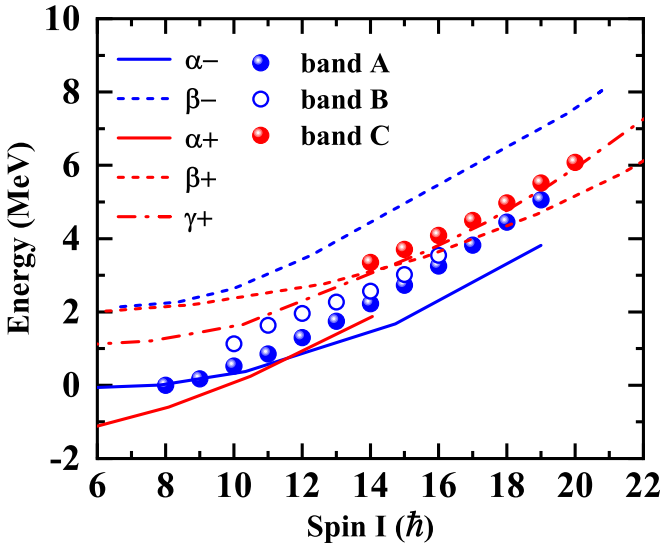

FIG. 9. Calculated rotational energies as a function of the angular momenta in comparison with the data.

and $\gamma+$. Two negative-parity configurations are labeled as $\alpha-$ and $\beta-$.

The energy spectra based on these configurations are shown in Fig. 9 in comparison with the experimental data. For the negative-parity band A, the configuration $\beta-$ can be excluded because its energy is too high. The possible configuration is $\alpha-$. At the rotational frequency $\hbar\omega = 0.0$ MeV, the alignment of the valence neutrons in $(g_{7/2}, d_{5/2})$ orbits of $\alpha-$ is roughly zero, indicating they are fully paired. As the rotational frequency increases, two of the valence neutrons in $(g_{7/2}, d_{5/2})$ orbits align toward each other and contribute an angular momentum of roughly $6\hbar$ at the rotational frequency $\hbar\omega = 0.4$ MeV ($I \approx 12\hbar$). There is no proper configuration for band B in the present calculations. Considering the fact that bands A and B are lying close to each other, band B might be a chiral partner band of band A.

To justify the chiral nature of bands A and B, the magnitude of triaxial deformation and the orientation angles θ and ϕ of the total angular momentum $\boldsymbol{J}$ in the intrinsic frame are examined. The obtained results are very similar to its neighboring odd-odd nucleus ^{106}Ag [53]. In Fig. 10(a), the potential energy surface of ^{104}Ag at the rotational frequency $\hbar\omega = 0.4$ MeV is shown with the configuration fixed to $\alpha-$. Although the triaxial deformation is only $\gamma \approx 5^\circ$ at the minimum, the potential energy surface is soft in the triaxial direction; the energy rise is less than 1.5 MeV with the change in triaxial deformation of 22°. For the orientation angles of the total angular momentum $\boldsymbol{J}$ in the intrinsic frame, the polar angle θ varies from 64° to 80° driven by the increasing rotational frequency from 0.1 to 0.6 MeV, while the azimuthal angle ϕ vanishes at all rotational frequencies. Although this corresponds to a planar rotation, the angular momentum $\boldsymbol{J}$ can execute a quantal motion, oscillating around the planar equilibrium into the left- and right-handed sectors, which leads to the so-called chiral vibration. The experimental observation of chiral vibration requires a relatively low vibrational energy, which in turn requires a slow rise in the Routhian curve along the ϕ degree of freedom. In Fig. 10(b), the total Routhian curve at rotational frequency $\hbar\omega = 0.4$ MeV for the configuration $\alpha-$ is shown as a function of the azimuthal angle ϕ_ω of the angular velocity $\boldsymbol{\omega}$. It can be seen that the Routhian grows very slowly with the increasing ϕ_ω, rising only several tens of keV from $\phi_\omega = 0^\circ$ to 30°. This indicates that the chiral vibration around the planar equilibrium into the left- and right-handed sectors should be substantial, and a pair of chiral vibrational bands can be generated based on the configuration $\alpha-$.

Amongst the positive-parity configurations, $\alpha+$ corresponds to the low-lying states with single-particle nature as suggested in Ref. [18]. Both configurations $\beta+$ and $\gamma+$ are possible for band C from the energy spectra and the final result needs help from the angular momenta and $B(M1)$ results in Fig. 11.

The angular momentum vs rotational frequency and $B(M1)$ vs spin curves for configurations $\alpha-$, $\beta+$, and $\gamma+$ are also compared with the data as shown in Fig. 11. The calculated

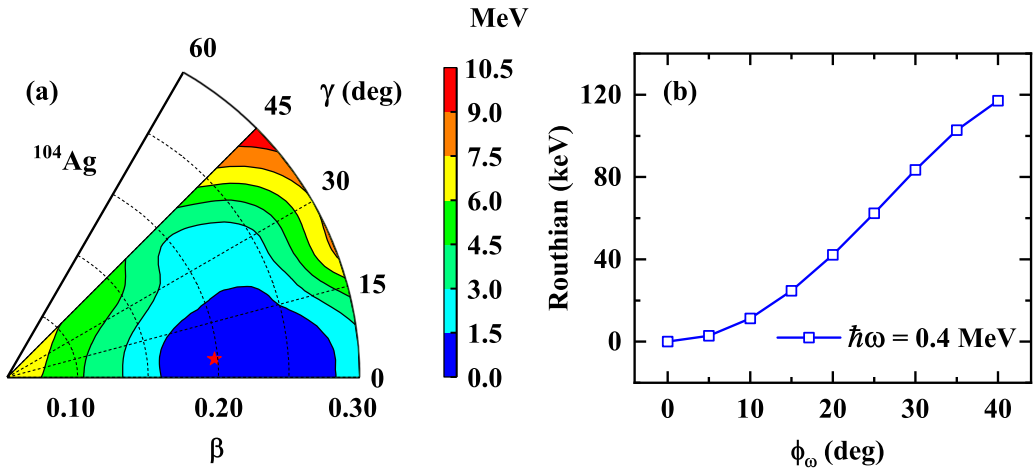

FIG. 10. Potential energy surface in the β-γ deformation plane (left) and total Routhian curve as a function of the azimuthal angle ϕ_ω of the angular velocity $\boldsymbol{\omega}$ (right) for the configuration $\pi g_{9/2}^{-1} \otimes \nu h_{11/2}(gd)^2$ at the rotational frequency $\hbar\omega = 0.4$ MeV. The star denotes the position of the minimum energy in the potential energy surface. The Routhian curve is renormalized to its minima at $\phi_\omega = 0^\circ$.

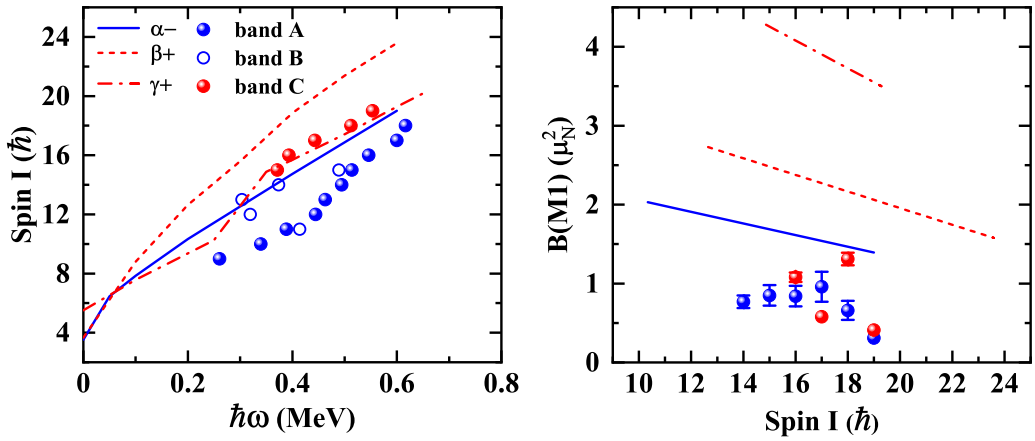

FIG. 11. The angular momentum as a function of rotational frequency and $B(M1)$ as a function of spin for configurations $\alpha-$, $\beta+$, and $\gamma+$ in comparison with the data.

angular momenta and $B(M1)$ values based on $\alpha-$ reproduce the data reasonably well, thus the configuration assignment to bands A and B is validated. For band C, the angular momenta and $B(M1)$ values are reproduced well based on the configuration $\beta+$. Even though the calculated angular momenta based on $\gamma+$ reproduce the data satisfactorily, $\gamma+$ should be excluded because it strongly overestimates the $B(M1)$ values. The theoretically suggested configuration is consistent with the one suggested in Ref. [19]; however, the deformation parameters predicted from present calculations are $\beta = 0.24$ and $\gamma = 7.5^\circ$ while in Ref. [19] it was suggested to be $\beta = 0.18$ and $\gamma = 25^\circ$.

The quasiparticle alignments of bands A and B can be compared with those of bands 1–3 from the neighboring odd-odd nucleus ^{106}Ag [17,53] as shown in Fig. 12. The configuration of band A can be assigned as $\pi g_{9/2}^{-1} \otimes \nu h_{11/2}$ at low spins and as $\pi g_{9/2}^{-1} \otimes \nu h_{11/2}(gd)^2$ at high spins. The configuration of band B can be assigned as $\pi g_{9/2}^{-1} \otimes \nu h_{11/2}(gd)^2$. Bands A and B are probably chiral doublet bands based on $\pi g_{9/2}^{-1} \otimes \nu h_{11/2}(gd)^2$, similar to the bands 2 and 3 in ^{106}Ag.

Experimentally, there are a few relatively strong $E1$ transitions connecting the positive-parity band and the yrast negative-parity band. To explore the octupole correlations in ^{104}Ag, the potential energy surface in the β_{20}-β_{30} plane for the ground state of ^{104}Ag is calculated by CDFT in the 3D lattice and shown in Fig. 13. For the CDFT calculations, the step sizes along the x, y, and z axes are chosen as 1.0 fm. The grid numbers are 24 for the x and y axes and 28 for the z axis. The size of the space adopted here is sufficient to obtain converged solutions. Although the octupole deformation $\beta_{30} = 0^\circ$ at the minimum, the potential energy surface is rather soft in the octupole direction; the energy rise is less than 0.4 MeV with change in octupole deformation of 0.05. Similar to the interpretation for the chiral doublet bands with octupole correlations in ^{124}Cs [37] and ^{78}Br [66], the octupole soft nature predicted in ^{104}Ag is expected to be responsible

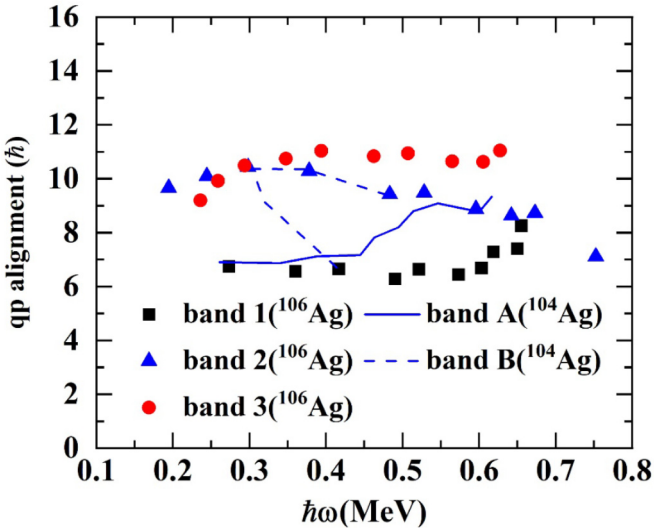

FIG. 12. Plot of the quasiparticle alignment as a function of spin for ^{104}Ag and ^{106}Ag. The Harries parameters used are $\mathrm{Im}_0 = 7.0\,\hbar^2/\mathrm{MeV}$ and $\mathrm{Im}_1 = 15.0\,\hbar^4/\mathrm{MeV}$ [46].

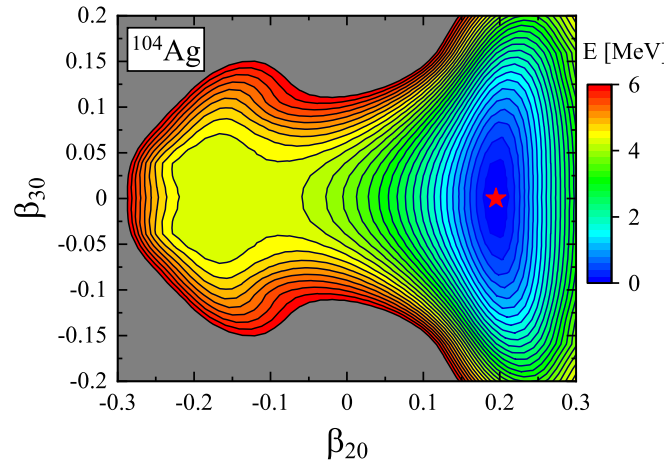

FIG. 13. The potential energy surface of ^{104}Ag calculated using 3D lattice CDFT. The energies are normalized to the ground state with $(\beta_{20}, \beta_{30}) = (0.195, 0.0)$. The contour separation is 0.2 MeV.

for the enhanced $E1$ transitions between the positive- and negative-parity bands.

V. SUMMARY

The high-spin structure in the ^{104}Ag nucleus has been investigated through the fusion evaporation reaction ^{76}Ge(^{32}S, $p3n$) at a beam energy of 110 MeV. In the present paper, lifetime measurements have been done for various states in the negative-parity yrast band and positive-parity magnetic rotational band at an excitation energy of 4424 keV. Lifetimes of seven states and upper limits on lifetimes of three states were obtained using the DSAM technique. Lifetimes of three states (17^-, 18^-, and 19^-) of the yrast band and the 16^+ state of the positive band based on 4424 keV have been determined for the first time. In the case of states where lifetimes have been known from earlier studies, the errors have been reduced significantly. From our directional correlation measurements of gamma rays (DCO) we have also been able to confirm some of the spin-parity assignments which were tentatively assigned before. We have observed enhanced $E1$ transitions (three known from earlier studies and two more from the present paper) from the positive-parity band based on 4424 keV to the yrast and its proposed (from earlier study) chiral partner band. We have performed calculations based on TPSM and CDFT approaches to understand the above mentioned band structures. It is evident from the presented results that TPSM provides a reasonable description of all the properties of the two observed negative-parity bands. Further, it has been shown that two bands have finite angular momentum projections along the three principle axes, which indicates that two bands could be associated with the chiral symmetry breaking. The CDFT calculations suggest assignment of $\pi g_{9/2}^{-1} \otimes \nu h_{11/2}$ for the yrast band and above spin of the $\approx 12\hbar$, $\pi(g_{9/2})^{-1} \otimes \nu(h_{11/2})(g_{7/2}, d_{5/2})^2$ aligned quasiparticle configuration for the yrast and the partner band. The deformations predicted for the yrast and the partner band are $\beta \approx 0.20$ and $\gamma \approx 5^\circ$ at higher spins. The partner band can be thought to be a chiral vibrational mode built on top of the yrast band. The positive-parity band based on the 4424-keV state is predicted to have the $\pi(g_{9/2})^{-1} \otimes \nu(h_{11/2})^2(g_{7/2}, d_{5/2})^1$ aligned quasiparticle configuration. The potential energy surface calculation based on CDFT predicts significant softness with respect to octupole deformation and this could be the reason for the enhanced $E1$ transitions from the above positive-parity band to the yrast and its chiral partner band. This is analogous to the octupole correlations observed along with chiral doublet bands in ^{78}Br and ^{124}Cs.

ACKNOWLEDGMENTS

We would like to acknowledge BARC-TIFR pelletron staff for delivering a stable beam of ^{32}S during the experiment. We acknowledge the help of the INGA collaboration. We gratefully acknowledge the Department of Science and Technology (Government of India) for INGA Project No. IR/S2/PF-30/2003-II. This work was supported by the Department of Atomic Energy, Government of India (Project No. RTI 4002). K.K. acknowledges a CSIR research grant (Grant No. 09/760(0032)/2017-EMR-I) for financial support. This work was supported by the U.S. National Science Foundation (Grants No. PHY-1068192 and No. PHY-2011890) and by the APS-IUSSTF Physics Student and Post-Doc Visitation Program. S.J., G.H.B., N.R., and J.A.S. acknowledge the Science and Engineering Research Board, Department of Science and Technology (Government of India) for providing financial assistance under Project No. CRG/2019/004960 to carry out a part of the present research work. We would also like to thank R. Bhattacharjee, S. S. Bhattacharjee, S. Samanta, S. Das, N. Ghosh, A. K. Sinha, S. Mukhopadhyay, L. Dhanu, B. K. Nayak, D. C. Biswas, A. Y. Deo, S. K. Tandel, N. Kaur, Ashok Kumar, J. Sethi, and S. Chattopadhyay for their initial involvement in the project. Fruitful discussions with J. Meng and Z. X. Ren on the theoretical interpretation are also acknowledged. A special thanks goes to Prof. S. C. Pancholi for his unconditional guidance.

[1] S. Frauendorf, Nucl. Phys. A **557**, 259 (1993).
[2] R. M. Clark and A. O. Macchiavelli, Annu. Rev. Nucl. Part. Sci. **50**, 1 (2000).
[3] H. Hübel, Prog. Part. Nucl. Phys. **54**, 1 (2005).
[4] S. Frauendorf, Rev. Mod. Phys. **73**, 463 (2001).
[5] S. Frauendorf and J. Meng, Nucl. Phys. A **617**, 131 (1997).
[6] P. Joshi, D. G. Jenkins, P. M. Raddon, A. J. Simons, R. Wadsworth, A. R. Wilkinson, D. B. Fossan, T. Koike, K. Starosta, C. Vaman, J. Timór, Z. Dombródi, A. Krasznahorkay, J. Molnór, D. Sohler, L. Zolnai, A. Algora, E. S. Paul, G. Rainovski, A. Gizon *et al.*, Phys. Lett. B **595**, 135 (2004).
[7] C. Vaman, D. B. Fossan, T. Koike, K. Starosta, I. Y. Lee, and A. O. Macchiavelli, Phys. Rev. Lett. **92**, 032501 (2004).
[8] T. Suzuki, G. Rainovski, T. Koike, T. Ahn, M. P. Carpenter, A. Costin, M. Danchev, A. Dewald, R. V. F. Janssens, P. Joshi, C. J. Lister, O. Möller, N. Pietralla, T. Shinozuka, J. Timár, R. Wadsworth, C. Vaman, and S. Zhu, Phys. Rev. C **78**, 031302(R) (2008).
[9] J. Timar, C. Vaman, K. Starosta, D. B. Fossan, T. Koike, D. Sohler, I. Y. Lee, and A. O. Macchiavelli, Phys. Rev. C **73**, 011301(R) (2006).
[10] P. Joshi, M. P. Carpenter, D. B. Fossan, T. Koike, E. S. Paul, G. Rainovski, K. Starosta, C. Vaman, and R. Wadsworth, Phys. Rev. Lett. **98**, 102501 (2007).
[11] T. Koike, K. Starosta, C. J. Chiara, D. B. Fossan, and D. R. LaFosse, Phys. Rev. C **67**, 044319 (2003).
[12] W. Shou-Yu, Z. Shuang-Quan, Q. Bin, and M. Jie, Chin. Phys. Lett. **24**, 664 (2007).
[13] D. Tonev, G. de Angelis, S. Brant, S. Frauendorf, P. Petkov, A. Dewald, F. Dönau, D. L. Balabanski, Q. Zhong, P. Pejovic, D. Bazzacco, P. Bednarczyk, F. Camera, D. Curien, F. Della Vedova, A. Fitzler, A. Gadea, G. Lo Bianco, S. Lenzi, S. Lunardi *et al.*, Phys. Rev. C **76**, 044313 (2007).
[14] D. Tonev, M. S. Yavahchova, N. Goutev, G. de Angelis, P. Petkov, R. K. Bhowmik, R. P. Singh, S. Muralithar, N. Madhavan, R. Kumar, M. K. Raju, J. Kaur, G. Mohanto,

A. Singh, N. Kaur, R. Garg, A. Shukla, Ts. K. Marinov, and S. Brant, Phys. Rev. Lett. **112**, 052501 (2014).
[15] E. Grodner, I. Sankowska, T. Morek, S. G. Rohoziński, C. Droste, J. Srebrny, A. A. Pasternak, M. Kisieliński, M. Kowalczyk, J. Kownacki, J. Mierzejewski, A. Król, and K. Wrzosek, Phys. Lett. B **703**, 46 (2011).
[16] E. Grodner, J. Srebrny, A. A. Pasternak, I. Zalewska, T. Morek, Ch. Droste, J. Mierzejewski, M. Kowalczyk, J. Kownacki, M. Kisieliński, S. G. Rohoziński, T. Koike, K. Starosta, A. Kordyasz, P. J. Napiorkowski, M. Wolińska-Cichocka, E. Ruchowska, W. Płóciennik, and J. Perkowski, Phys. Rev. Lett. **97**, 172501 (2006).
[17] E. O. Lieder, R. M. Lieder, R. A. Bark, Q. B. Chen, S. Q. Zhang, J. Meng, E. A. Lawrie, J. J. Lawrie, S. P. Bvumbi, N. Y. Kheswa, S. S. Ntshangase, T. E. Madiba, P. L. Masiteng, S. M. Mullins, S. Murray, P. Papka, D. G. Roux, O. Shirinda, Z. H. Zhang, P. W. Zhao *et al.*, Phys. Rev. Lett. **112**, 202502 (2014).
[18] Z. G. Wang, M. L. Liu, Y. H. Zhang, X. H. Zhou, B. T. Hu, N. T. Zhang, S. Guo, B. Ding, Y. D. Fang, J. G. Wang, G. S. Li, Y. H. Qiang, S. C. Li, B. S. Gao, Y. Zheng, W. Hua, X. G. Wu, C. Y. He, Y. Zheng, C. B. Li *et al.*, Phys. Rev. C **88**, 024306 (2013).
[19] P. Datta, S. Chattopadhyay, P. Banerjee, S. Bhattacharya, B. Dasmahapatra, T. K. Ghosh, A. Goswami, S. Pal, M. S. Sarkar, S. Sen, H. C. Jain, P. K. Joshi, and Amita, Phys. Rev. C **69**, 044317 (2004).
[20] W. A. Dar, J. A. Sheikh, G. H. Bhat, R. Palit, R. N. Ali, and S. Frauendorf, Nucl. Phys. A **933**, 123 (2015).
[21] R. Palit, S. Saha, J. Sethi, T. Trivedi, S. Sharma, B. S. Naidu, S. Jadhav, R. Donthi, P. B. Chavan, H. Tan, and W. Hennig, Nucl. Instrum. Methods Phys. Res. Sect. A **680**, 90 (2012).
[22] D. C. Radford, Nucl. Instrum. Methods Phys. Res. Sect. A **361**, 297 (1995).
[23] D. C. Radford, Nucl. Instrum. Methods Phys. Res. Sect. A **361**, 306 (1995).
[24] K. S. Krane, R. M. Steffen, and R. M. Wheeler, At. Data Nucl. Data Tables **11**, 351 (1973).
[25] J. Tréherne, J. Genevey, S. André, R. Béraud, A. Charvet, R. Duffait, A. Emsallem, M. Meyer, C. Bourgeois, P. Kilcher, J. Sauvage, F. A. Beck, and T. Byrski, Phys. Rev. C **27**, 166 (1983).
[26] J. C. Wells and N. R. Johnson, ORNL Report No. ORNL-6689, 1991 (unpublished), p. 44.
[27] S. Das, S. Samanta, R. Bhattacharjee, R. Raut, S. S. Ghugre, A. K. Sinha, U. Garg, R. Chakrabarti, S. Mukhopadhyay, A. Dhal, M. Kumar Raju, N. Madhavan, S. Muralithar, R. P. Singh, K. Suryanarayana, P. V. Madhusudhana Rao, R. Palit, S. Saha, and J. Sethi, Nucl. Instrum. Methods Phys. Res. Sect. A **841**, 17 (2017).
[28] www.srim.org.
[29] A. Sharma, R. Raut, S. Muralithar, R. P. Singh, S. S. Bhattacharjee, S. Das, S. Samanta, S. S. Ghugre, R. Palit, S. Jehangir, N. Rather, G. H. Bhat, J. A. Sheikh, S. S. Tiwary, Neelam, P. V. Madhusudhana Rao, U. Garg, and S. K. Dhiman, Phys. Rev. C **103**, 024324 (2021).
[30] T. K. Alexander and J. S. Forster, Adv. Nucl. Phys. **10**, 197 (1978).
[31] C. Y. He, L. H. Zhu, X. G. Wu, S. X. Wen, G. S. Li, Y. Liu, Z. M. Wang, X. Q. Li, X. Z. Cui, H. B. Sun, R. G. Ma, and C. X. Yang, Phys. Rev. C **81**, 057301 (2010).
[32] C. Liu, S. Y. Wang, B. Qi, D. P. Sun, C. J. Xu, L. Liu, B. Wang, X. C. Shen, M. R. Qin, H. Chen, L. H. Zhu, X. G. Wu, G. S. Li, C. Y. He, Y. Zheng, L. L. Wang, B. Zhang, G. Y. Liu, and Y. W. Wang, Int. J. Mod. Phys. E **20**, 2351 (2011).
[33] G. de Angelis, C. Fahlander, A. Gadea, E. Farnea, D. Bazzacco, N. Belcari, N. Blasi, P. G. Bizzeti, A. Bizzeti-Sona, D. de Acuña, M. D. Poli, H. Grawe, A. Johnson, G. L. Bianco, S. Lunardi, D. R. Napoli, J. Nyberg, P. Pavan, J. Persson, C. R. Alvarez *et al.*, Phys. Lett. B **437**, 236 (1998).
[34] G. J. Lane, D. B. Fossan, J. M. Sears, J. F. Smith, J. A. Cameron, R. M. Clark, I. M. Hibbert, V. P. Janzen, R. Krücken, I.-Y. Lee, A. O. Macchiavelli, C. M. Parry, and R. Wadsworth, Phys. Rev. C **57**, R1022(R) (1998).
[35] G. de Angelis, A. Gadea, E. Farnea, R. Isocrate, P. Petkov, N. Marginean, D. R. Napoli, A. Dewald, M. Bellato, A. Bracco, F. Camera, D. Curien, M. De Poli, E. Fioretto, A. Fitzler, S. Kasemann, N. Kintz, T. Klug, S. Lenzi, S. Lunardi *et al.*, Phys. Lett. B **535**, 93 (2002).
[36] Z. Liu, X. Sun, X. Zhou, X. Lei, Y. Guo, Y. Zhang, X. Chen, H. Jin, Y. Luo, S. X. Wen, C. X. Yang, G. J. Yuan, G. S. Li, X. A. Liu, W. D. Luo, and Y. S. Chen, Eur. Phys. J. A **1**, 125 (1998).
[37] K. Selvakumar, A. K. Singh, C. Ghosh, P. Singh, A. Goswami, R. Raut, A. Mukherjee, U. Datta, P. Datta, S. Roy, G. Gangopadhyay, S. Bhowal, S. Muralithar, R. Kumar, R. P. Singh, and M. K. Raju, Phys. Rev. C **92**, 064307 (2015).
[38] P. Mason, G. Benzoni, A. Bracco, F. Camera, B. Million, O. Wieland, S. Leoni, A. K. Singh, A. A. Khatib, H. Hubel, P. Bringel, A. Burger, A. Neusser, G. Schonwasser, B. M. Nyako, J. Timar, A. Algora, Z. Dombradi, J. Gal, G. Kalinka *et al.*, Phys. Rev. C **72**, 064315 (2005).
[39] J. A. Sheikh, G. H. Bhat, W. A. Dar, S. Jehangir, and P. A. Ganai, Phys. Scr. **91**, 063015 (2016).
[40] S. Jehangir, G. H. Bhat, N. Rather, J. A. Sheikh, and R. Palit, Phys. Rev. C **104**, 044322 (2021).
[41] S. Jehangir, I. Maqbool, G. H. Bhat, J. A. Sheikh, R. Palit, and N. Rather, Eur. Phys. J. A **56**, 197 (2020).
[42] G. H. Bhat, J. A. Sheikh, W. A. Dar, S. Jehangir, R. Palit, and P. A. Ganai, Phys. Lett. B **738**, 218 (2014).
[43] G. H. Bhat, J. A. Sheikh, and R. Palit, Phys. Lett. B **707**, 250 (2012).
[44] P. Moller, J. R. Nix, W. D. Myers, and W. J. Swiatecki, At. Data Nucl. Data Tables **59**, 185 (1995).
[45] P. Ring and P. Schuck, *The Nuclear Many-Body Problem* (Springer-Verlag, Berlin, 1980).
[46] P. H. Regan, A. E. Stuchbery, G. D. Dracoulis, A. P. Byrne, G. J. Lane, T. Kibédi, D. C. Radford, A. Galindo-Uribarri, V. P. Janzen, D. Ward, S. M. Mullins, G. Hackman, J. H. DeGraaf, M. Cromaz, and S. Pilotte, Nucl. Phys. A **586**, 351 (1995).
[47] A. I. Levon, J. de Boer, A. A. Pasternak, and D. A. Volkov, Z. Phys. A - Hadrons Nuclei **343**, 131 (1992).
[48] B. M. Musangu, E. H. Wang, J. H. Hamilton, S. Jehangir, G. H. Bhat, J. A. Sheikh, S. Frauendorf, C. J. Zachary, J. M. Eldridge, A. V. Ramayya, A. C. Dai, F. R. Xu, J. O. Rasmussen, Y. X. Luo, G. M. Ter-Akopian, Y. T. Oganessian, and S. J. Zhu, Phys. Rev. C **104**, 064318 (2021).
[49] P. Ring, Prog. Part. Nucl. Phys. **37**, 193 (1996).
[50] *Relativistic Density Functional for Nuclear Structure*, edited by J. Meng, International Review of Nuclear Physics Vol. 10 (World Scientific, Singapore, 2016).
[51] J. Meng and P. Zhao, AAPPS Bull. **31**, 2 (2021).
[52] P. W. Zhao, Phys. Lett. B **773**, 1 (2017).
[53] P. W. Zhao, Y. K. Wang, and Q. B. Chen, Phys. Rev. C **99**, 054319 (2019).

[54] C. M. Petrache, B. F. Lv, A. Astier, E. Dupont, Y. K. Wang, S. Q. Zhang, P. W. Zhao, Z. X. Ren, J. Meng, P. T. Greenlees, H. Badran, D. M. Cox, T. Grahn, R. Julin, S. Juutinen, J. Konki, J. Pakarinen, P. Papadakis, J. Partanen, P. Rahkila *et al.*, Phys. Rev. C **97**, 041304(R) (2018).

[55] Z. X. Ren, S. Q. Zhang, and J. Meng, Phys. Rev. C **95**, 024313 (2017).

[56] Z. X. Ren, S. Q. Zhang, P. W. Zhao, N. Itagaki, J. A. Maruhn, and J. Meng, Sci. China-Phys. Mech. Astron. **62**, 112062 (2019).

[57] Z. X. Ren, P. W. Zhao, S. Q. Zhang, and J. Meng, Nucl. Phys. A **996**, 121696 (2020).

[58] P. W. Zhao, Z. P. Li, J. M. Yao, and J. Meng, Phys. Rev. C **82**, 054319 (2010).

[59] K. Zhang, M.-K. Cheoun, Y.-B. Choi, P. S. Chong, J. Dong, L. Geng, E. Ha, X. He, C. Heo, M. C. Ho, E. J. In, S. Kim, Y. Kim, C.-H. Lee, J. Lee, Z. Li, T. Luo, J. Meng, M.-H. Mun, Z. Niu *et al.*, Phys. Rev. C **102**, 024314 (2020).

[60] Y. L. Yang, Y. K. Wang, P. W. Zhao, and Z. P. Li, Phys. Rev. C **104**, 054312 (2021).

[61] K. Zhang, M.-K. Cheoun, Y.-B. Choi, P. S. Chong, J. Dong, Z. Dong, X. Du, L. Geng, E. Ha, X.-T. He, C. Heo, M. C. Ho, E. J. In, S. Kim, Y. Kim, C.-H. Lee, J. Lee, H. Li, Z. Li, T. Luo *et al.*, At. Data Nucl. Data Tables **144**, 101488 (2022).

[62] P. W. Zhao, J. Peng, H. Z. Liang, P. Ring, and J. Meng, Phys. Rev. Lett. **107**, 122501 (2011).

[63] P. W. Zhao, S. Q. Zhang, J. Peng, H. Z. Liang, P. Ring, and J. Meng, Phys. Lett. B **699**, 181 (2011).

[64] J. Meng and P. Zhao, Phys. Scr. **91**, 053008 (2016).

[65] J. Meng, J. Peng, S. Q. Zhang, and S.-G. Zhou, Phys. Rev. C **73**, 037303 (2006).

[66] C. Liu, S. Y. Wang, R. A. Bark, S. Q. Zhang, J. Meng, B. Qi, P. Jones, S. M. Wyngaardt, J. Zhao, C. Xu, S.-G. Zhou, S. Wang, D. P. Sun, L. Liu, Z. Q. Li, N. B. Zhang, H. Jia, X. Q. Li, H. Hua, Q. B. Chen *et al.*, Phys. Rev. Lett. **116**, 112501 (2016).